*High Power Laser Science and Engineering*, (2024), Vol. 12, e31, 6 pages.
doi:10.1017/hpl.2024.12

HIGH POWER LASER SCIENCE AND ENGINEERING

RESEARCH ARTICLE

# Theory of small-scale self-focusing of spatially partially coherent beams and its implications for high-power laser systems

Ruifeng Wang[1,2], Xiaoqi Zhang[1], Yanli Zhang[1], Fanglun Yang[1], Jianhao Tang[1], Ziang Chen[1,2], and Jianqiang Zhu[1]

[1] *Key Laboratory of High Power Laser and Physics, Shanghai Institute of Optics and Fine Mechanics, Chinese Academy of Sciences, Shanghai, China*

[2] *Center of Materials Science and Optoelectronics Engineering, University of Chinese Academy of Sciences, Beijing, China*

*(Received 14 December 2023; revised 5 February 2024; accepted 22 February 2024)*

**Abstract**

Based on the paraxial wave equation, this study extends the theory of small-scale self-focusing (SSSF) from coherent beams to spatially partially coherent beams (PCBs) and derives a general theoretical equation that reveals the underlying physics of the reduction in the B-integral of spatially PCBs. From the analysis of the simulations, the formula for the modulational instability (MI) gain coefficient of the SSSF of spatially PCBs is obtained by introducing a decrease factor into the formula of the MI gain coefficient of the SSSF of coherent beams. This decrease can be equated to a drop in the injected light intensity or an increase in the critical power. According to this formula, the reference value of the spatial coherence of spatially PCBs is given, offering guidance to overcome the output power limitation of the high-power laser driver due to SSSF.

**Keywords:** B-integral; complex screen method; nonlinearity; small-scale self-focusing; spatially partially coherent beams

## 1. Introduction

High-power neodymium-glass laser drivers have become the worldwide system of choice for laser fusion research[1,2]. They serve as a crucial platform for research in high-energy-density physics[3], such as X-ray generation, laser plasma physics[4] and laboratory astrophysics. Following propagation in a nonlinear medium, a high-power laser undergoes whole-beam self-focusing (WBSF) and small-scale self-focusing (SSSF) owing to third-order nonlinear polarization; the latter is more destructive[5–7]. The Bespalov–Talanov (B-T) theory provides an explanation for the SSSF of coherent beams[8]. The well-known B-integral characterizes the growth rate of small-scale modulation in high-power Nd:glass lasers. In the 1970s, Campillo *et al.*[9] and Bliss *et al.*[10] examined the B-T theory. The results of the experiment demonstrated that SSSF affected the beam quality[11], induced catastrophic damage to the laser medium and optical components and constrained the laser system output power.

Several methods for self-focusing suppression delay the onset of SSSF and increase the output power. Common techniques include using soft-edged apertures for apodization[12], using broadband chirped pulses[13], divergent beams[14,15], circularly polarized beams[16] and spatially partially coherent beams (PCBs)[17], using spatial filters[18] and a medium with negative nonlinear coefficients[19]. PCBs in the temporal domain have been developed for laser drivers due to their ability to reduce nonlinear effects, such as chirps, and improve the uniformity of the optical field[20,21]. PCBs in the spatial domain have proven to be efficient in suppressing speckles caused by spatial coherence, such as optical imaging, particle trapping and image transmission in the linear regime[22–29]. In the nonlinear regime[30,31], WBSF of spatially PCBs was studied by Hunt *et al.* in 1978[32]. We believe that reducing the spatial coherence of high-power laser systems can suppress SSSF of spatially PCBs and reduce the value of the B-integral. Determining the relationship between spatial coherence and the growth rate of SSSF is the goal of this study.

Correspondence to: Xiaoqi Zhang, Yanli Zhang and Jianqiang Zhu, Key Laboratory of High Power Laser and Physics, Shanghai Institute of Optics and Fine Mechanics, Chinese Academy of Sciences, Shanghai 201800, China. Email: skcheung@siom.ac.cn (X. Zhang); zhangyl@siom.ac.cn (Y. Zhang); jqzhu@siom.ac.cn (J. Zhu)

There are numerous methods to spatially synthesize PCBs; three are commonly used. The first method constructs an optical field using the angular power spectrum[33,34]. The second method uses the van Cittert–Zernike theorem to produce arbitrary genuine PCBs of the Schell-model type by propagating a completely incoherent field distribution generated at a plane with a given intensity distribution[35–37]. The third method exploits the mode superposition principle, which includes coherent-mode representation, pseudo-mode representation and random-mode representation (mainly referring to the complex screen (CS) and phase screen (PS) methods). The CS method was developed because it can provide spatially PCBs without analytical expressions[38]. Basu *et al.*[39] used the CS method to represent Gaussian Schell-model beams in 2014. Wang *et al.*[40] expanded this method in 2022 to simulate time-domain PCBs transmitted in a nonlinear medium with an arbitrary correlation function, and verified its correctness by comparing it with the pulse-by-pulse method proposed by Lajunen *et al.* in 2010[41]. Yang *et al.*[42] used this method in 2023 to simulate the nonlinear transmission of Gaussian Schell-model beams. In this study, we chose the CS method to synthesize spatially PCBs.

As the SSSF of PCBs has recently been a subject of considerable interest, a theory of the SSSF of PCBs must be developed. We derived a theoretical equation for the SSSF of spatially PCBs to analyze their B-integral decrease and demonstrated the findings through simulations of the small-scale modulational instability (MI) gain coefficient with different degrees of spatial coherence. The results showed that the gain coefficient of the SSSF of spatially PCBs decreases compared to that of coherent beams. We extended the formula for the small-scale MI gain coefficient of coherent beams to spatially PCBs using a decrease factor that represents the effect of the spatial coherence of the beams on the SSSF. The decrease factor is closely related to the line shape and spatial coherence length of the correlation function. This study may promote an emerging high-power spatially partially coherent laser architecture to suppress the SSSF due to the Kerr effect, and provide valuable guidance for designing the seed source and assessing the load capacity.

## 2. Equation of small-scale self-focusing of spatially partially coherent beams and the complex screen method to synthesize spatially partially coherent beams

The analyzed spatially PCBs were quasi-monochromatic with a temporal coherence length that was much larger than the spatial coherence length. Here we focus on laser-induced breakdown with nanosecond pulse duration in the high peak power Nd:glass laser system. The response time of the Nd:glass was significantly shorter than the pulse duration and the coherence time, allowing the self-focusing to be steady-state self-focusing.

The nonlinear wave equation in paraxial approximation[8] has the following form:

$$\nabla_{\perp}^{2}E+2jk\frac{\partial E}{\partial z}=-k^{2}\left(\frac{n_{2}|E|^{2}}{n_{0}}\right)E, \tag{1}$$

where $\left|\frac{\partial^{2}E}{\partial z^{2}}\right| << k\left|\frac{\partial E}{\partial z}\right|$; $\nabla_{\perp}^{2}$ is the transverse Laplacian; $n_0$ denotes the linear refractive index; $n_2$ is the nonlinear refractive index; $k$ is the wave vector in the medium. Equation (1) includes the diffraction term $\nabla_{\perp}^{2}E$ and the nonlinear term $-k^{2}\left(\frac{n_{2}|E|^{2}}{n_{0}}\right)E$. This equation serves as a foundation for investigating the SSSF of spatially PCBs.

The modulated optical field $E$ can be described by linear superposition of a strong background field $T$ (infinite plane waves with arbitrary spatial coherence) with finite small-scale perturbation fields[2]:

$$E=T\left(x,y,z=0\right)\left(1+\sum_{i}u_{i}(z)e_{i}\left(x,y\right)\right), \tag{2}$$

where $u_i(z)e_i\left(x,y\right) << 1$, $u_i(z)=a(z)+ib(z)$, and both $T$ and $E$ satisfy Equation (1)[2]. Substituting Equation (2) into Equation (1), we obtain Equation (3):

$$\begin{aligned}&\nabla_{\perp}^{2}e\left(x,y\right)\times Tu(z)+2jkTe\left(x,y\right)u(z)_{z}+2k^{2}\left(\frac{n_{2}|T|^{2}}{n_{0}}\right)\\&\times T\times\mathrm{Re}\left(u(z)e\left(x,y\right)\right)=-2u(z)\left(T_{x}e(x,y)_{x}+T_{y}e(x,y)_{y}\right),\end{aligned} \tag{3}$$

where $u(z)_{z}=\frac{\partial u(z)}{\partial z}$, $T_{x}=\frac{\partial T}{\partial x}$ and $T_{y}=\frac{\partial T}{\partial y}$. The left-hand side of Equation (3) is consistent with the SSSF equation of coherent theory. The right-hand side of Equation (3) is the underlying physics that produces the difference in SSSF between spatially PCBs and coherent beams, where $e(x,y)_{x}$, $e(x,y)_{y}$ and $u(z)$ are all associated with the modulation. Here, $T_x$ and $T_y$ are proportional to $\sqrt{G\left(v_{x},v_{y}\right)}$, and $G\left(v_{x},v_{y}\right)$ represents the power spectrum. When $G\left(v_{x},v_{y}\right)\rightarrow\delta\left(v_{x},v_{y}\right)$, Equation (3) is reduced to the equation for coherent beams. Thus, the SSSF is related to the light intensity and to the power spectrum (which indicates the spatial coherence of the beams) of the optical field for spatially PCBs.

We then introduced the CS method to synthesize spatially PCBs with different spatial coherence. The methodology is presented as follows.

The cross-spectral density (CSD) function can be expressed as follows:

$$W\left(\boldsymbol{r}_{1},\boldsymbol{r}_{2},z\right)=<T\left(\boldsymbol{r}_{1},z\right)T^{*}\left(\boldsymbol{r}_{2},z\right)>. \tag{4}$$

The brackets represent the time average over the response time of the medium, $\boldsymbol{r}=\widehat{\boldsymbol{x}}x+\widehat{\boldsymbol{y}}y$. If the statistical properties

https://doi.org/10.1017/hpl.2024.12 Published online by Cambridge University Press

of spatially PCBs are of the Schell-model type, we obtain the following:

$$W(\boldsymbol{r}_1,\boldsymbol{r}_2,z=0)=E_{\mathrm{c}}(\boldsymbol{r}_1)E_{\mathrm{c}}^{*}(\boldsymbol{r}_2)\mu(\boldsymbol{r}_1-\boldsymbol{r}_2), \tag{5}$$

where $E_{\mathrm{c}}(\boldsymbol{r})$ denotes the coherent part of the beam. According to the condition proposed by Gori *et al.*[43,44] for devising a genuine correlation function of PCBs, $\mu$ can be expressed as follows:

$$\mu(\boldsymbol{r}_1-\boldsymbol{r}_2)=\iint\sqrt{G(\boldsymbol{v}_1)}\sqrt{G(\boldsymbol{v}_2)}\delta(\boldsymbol{v}_1-\boldsymbol{v}_2)\times e^{-j\boldsymbol{r}_1\boldsymbol{v}_1}e^{-j\boldsymbol{r}_2\boldsymbol{v}_2}\mathrm{d}\boldsymbol{v}_1\mathrm{d}\boldsymbol{v}_2, \tag{6}$$

where $\boldsymbol{v}=\hat{\boldsymbol{x}}v_x+\hat{\boldsymbol{y}}v_y$, and $\delta(\boldsymbol{v}_1-\boldsymbol{v}_2)$ is the Dirac function, which can be expressed as follows:

$$\delta(\boldsymbol{v}_1-\boldsymbol{v}_2)=<R(\boldsymbol{v}_1)R(\boldsymbol{v}_2)^{*}>, \tag{7}$$

where $R(\boldsymbol{v})$ is a random complex function whose real and imaginary parts are independent, with unit variances and standard normal distributions. When $R(\boldsymbol{v})$ is refreshed, a new random optical field $T$ is generated. Substituting Equations (6) and (7) into Equation (5), the CSD function can be rearranged as follows:

$$W(\boldsymbol{r}_1,\boldsymbol{r}_2,z=0)\approx\frac{1}{N}\sum_{n=1}^{N}T_n(\boldsymbol{r}_1)T_n^{*}(\boldsymbol{r}_2), \tag{8}$$

with the following:

$$T(\boldsymbol{r})=E_{\mathrm{c}}(\boldsymbol{r})\times\varphi(\boldsymbol{r}), \tag{9}$$

$$\varphi(\boldsymbol{r})=\iint\sqrt{G(\boldsymbol{v})}R(\boldsymbol{v})e^{-i2\pi\boldsymbol{r}\boldsymbol{v}}\mathrm{d}\boldsymbol{v}. \tag{10}$$

The CSD function can be described by Equation (8) to obtain sufficient optical fields. Different $T(x,y,z)$ can be obtained by changing the spatial coherence lengths and line shapes of the correlation function $\mu$. Using the Fourier transform, we can compute the corresponding power spectrum $G(v_x,v_y)$ based on the spatially partially coherent optical fields $T(x,y,z)$.

## 3. Simulations

As Equation (3) is unsolvable analytically, we used the split-step Fourier method with the following parameters: $n_0=1.5$, $n_2=1.5\times10^{-13}$ (esu), $\lambda=1.053$ μm, $I_0=10$ GW/cm$^2$, propagation distance $L=2$ cm. The computational grid of $512\times512$ points corresponds to a physical size of 2 cm × 2 cm. The number of CSs was set as $1.1\times10^5$ and the spatial frequency $f$ was accompanied by a small-scale modulation at $z=0$ cm, where $a_0=0.01$, $b_0=0$ and $e(x,y)=\cos(2\pi\cdot f\cdot x)$. The MI gain coefficient of the SSSF was obtained by calculating the degree of modulation of the intensity distribution through the transmission. The amplitudes are satisfied as follows:

$$\frac{u(z)}{u(0)}=\frac{e^{gL}+e^{-gL}}{2}. \tag{11}$$

We simulated the impact on the MI gain coefficient $g$ by varying the spatial coherence lengths and line shapes of the correlation function $\mu$. Figure 1(a) demonstrates the 1D distributions of Gaussian correlation functions $\mu_{\mathrm{Gauss}}=e^{-\left(\frac{x^2+y^2}{2\sigma^2}\right)}$, where $\sigma$ is the spatial coherence length and the Bessel correlation function $\mu_{\mathrm{Bessel}}=J_1(2\pi\boldsymbol{v}\boldsymbol{r})$. We defined the spatial coherence length $\sigma_{\mathrm{Bessel}}$ as the value of the first zero of the Bessel function. Figure 1(b) demonstrates the corresponding power spectra, $G_{\mathrm{gauss}}$ and $G_{\mathrm{circle}}$, which satisfy the following:

$$G_{\mathrm{gauss}}(0,0)=G_{\mathrm{circle}}(0,0), \tag{12}$$

$$\iint G_{\mathrm{gauss}}(v_x,v_y)\mathrm{d}v_x\mathrm{d}v_y=\iint G_{\mathrm{circle}}(v_x,v_y)\mathrm{d}v_x\mathrm{d}v_y. \tag{13}$$

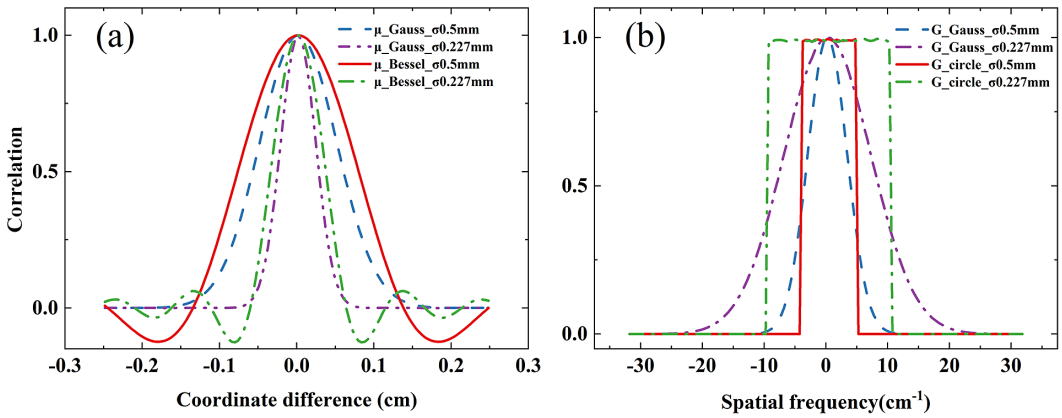


**Figure 1.** The correlation functions $\mu_{\mathrm{Gauss}}$ and $\mu_{\mathrm{Bessel}}$ are shown in (a) with different $\sigma$. The corresponding power spectra $G_{\mathrm{gauss}}$ and $G_{\mathrm{circle}}$ are shown in (b). Here, $\sigma=\sigma_{\mathrm{Gauss}}$ are 0.5 and 0.227 mm, respectively.

https://doi.org/10.1017/hpl.2024.12 Published online by Cambridge University Press

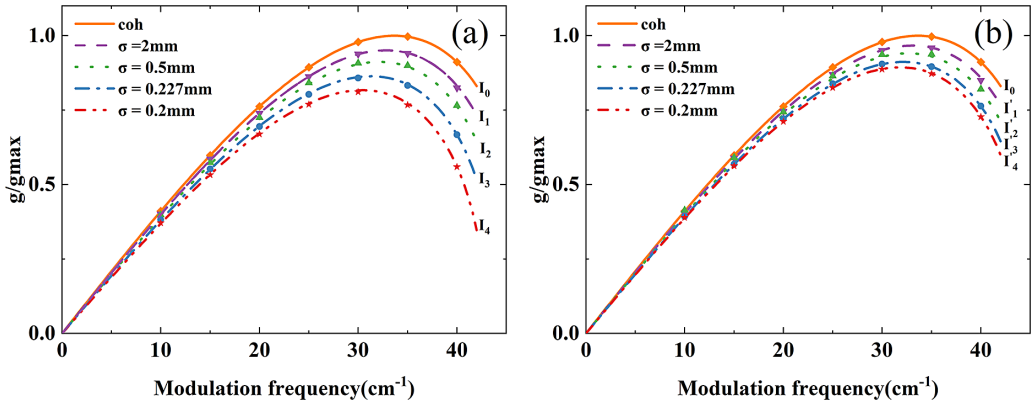


**Figure 2.** Analytical gain curves (lines) corresponding to different input intensities: (a) simulation results of the MI gain coefficient $g$ at different spatial coherence lengths when $\mu = \mu_{\text{Gauss}}$, $I_1 = 9.51$ GW/cm$^2$, $I_2 = 9.12$ GW/cm$^2$, $I_3 = 8.64$ GW/cm$^2$, $I_4 = 8.17$ GW/cm$^2$; (b) simulation results of the MI gain coefficient $g$ at different spatial coherence lengths when $\mu = \mu_{\text{Bessel}}$, $I_1' = 9.67$ GW/cm$^2$, $I_2' = 9.41$ GW/cm$^2$, $I_3' = 9.12$ GW/cm$^2$, $I_4' = 8.93$ GW/cm$^2$.

Equations (12) and (13) indicate that both power spectra exhibit the same maximum values and equal energy. Thus, we use $\sigma_{\text{Gauss}}$ uniformly to refer to $\sigma$ in the following.

We set $f$ = 10, 15, 20, 25, 30, 35, 40, and 42 cm$^{-1}$. In Figure 2(a), $\mu = \mu_{\text{Gauss}}$; in Figure 2(b), $\mu = \mu_{\text{Bessel}}$, and the simulations are displayed as data points, each point representing a result of the MI gain coefficient $g$ at the modulation frequency. The simulation results for the MI gain coefficient $g$ of the coherent beams fit well with the curves established using the analytical formula (solid line), indicating the correctness of the simulation. For the PCBs, the MI gain coefficients $g$ are consistently lower than those of the coherent beams, yet they exhibit a similar trend. Thus, we postulate that this is comparable to a reduction in the input intensity when injecting coherent beams. The remaining lines in Figure 2 represent the analytical gain curves of the MI gain coefficient $g$ of coherent beams with different injection intensities. As expected, the curves match the data points perfectly at 10 GW/cm$^2$ and other injection intensities, verifying the accuracy of the prediction. Thus, the formula for $g$ in coherent theory is extended to the following[45]:

$$g = \frac{|K|}{2k}\sqrt{\frac{2\pi I_0}{P_{\text{cr}}}\alpha - |K|^2}, \tag{14}$$

where $K = 2\pi \cdot f$; $P_{\text{cr}} = \frac{\lambda^2 c}{32\pi^2 n_2}$ is the critical power; $\alpha$ represents the decrease factor, $\alpha = 1$ for coherent beams and $\alpha < 1$ for spatially PCBs. Referring to Equation (14), we deduce the fastest growing frequency $K_{\max} = \sqrt{\frac{\pi I_0}{P_{\text{cr}}}\alpha}$ and the maximum gain coefficient $g_{\max} = \frac{\pi I_0}{2kP_{\text{cr}}}\alpha$ for PCBs. Equation (14) illustrates that the suppression effect of spatially PCBs for SSSF can be equated to a reduction in the injected light intensity or an increase in the critical power of coherent beams. Figure 3 compares the effect of the line shape and the spatial coherence length of the correlation function on

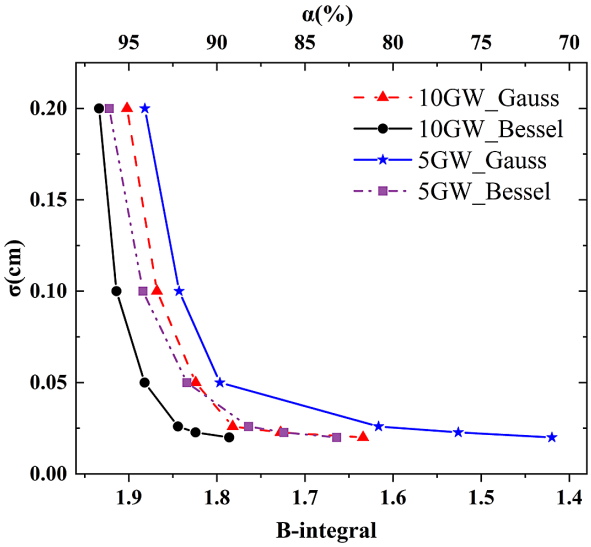


**Figure 3.** Variations in $\alpha$ and B-integral with respect to different light densities and correlation functions.

the decrease factor $\alpha$ and the B-integral for the same incident light intensity; it also compares the effect of the incident light intensity on the decrease factor $\alpha$ and the B-integral with the same spatial coherence. Experience has shown that the B-integral must be less than approximately 2 to avoid unacceptable small-scale modulation growth[46]. Thus, we set the B-integral of the coherent beams to 2 and $B = g_{\max}L$ without considering the gain of the medium. It is obvious from Figure 3 that the $\alpha$ corresponding to the Gaussian correlation function is smaller than that corresponding to the Bessel correlation function. This is because the spatially PCBs of the Gaussian correlation function have a wider power spectrum range when energy is conserved, implying that the larger the spatial divergence angle of the beams, the more rapidly the B-integral decreases and the better the suppression of SSSF. For the same spatial coherence length, the B-integral decreases more when the incident light

https://doi.org/10.1017/hpl.2024.12 Published online by Cambridge University Press

intensity is low, which means that to achieve the same SSSF suppression effect, the spatial coherence of the beam is much higher at a low light intensity than at a high light intensity. For the same spatial coherence, $\alpha$ decreases nonlinearly with incident intensities, which means the coupling between the spatial coherence and the incident light intensity of spatially PCBs. This conclusion is consistent with the physical nature revealed by Equation (3). To characterize the reference value of the spatial coherence of the beam, we used the ratio $\beta$ of the period of the fastest growing modulation to the spatial coherence length. For example, with an incident light intensity of 10 GW/cm$^2$, the B-integral decreasing rate began to accelerate significantly when $\beta$ was greater than 1.13, corresponding to a spatial coherence length of 0.26 mm. This result aligns consistently with diffraction by apertures illuminated with spatially PCBs[47].

## 4. Conclusion

This study has extended the theory of SSSF from coherent beams to spatially PCBs. The corresponding equation was derived based on a paraxial nonlinear wave equation. This equation indicated the underlying physics for the decrease in the B-integral of spatially PCBs. Using the numerical solutions of the equation, the formula for the MI gain coefficient of spatially PCBs was obtained by introducing a decrease factor into the formula for coherent beams. The decrease factor determined the maximum gain factor and the fastest growth frequency of the spatially PCBs; its influence on SSSF can be equated to a reduction in the injected light intensity or an increase in the critical power. Simulations of the variations in the decrease factor and B-integral were analyzed with respect to different spatial coherence lengths and different input light intensities. The results showed that the decrease factor was affected by the coupling of the source spatial coherence and the injected light intensity of the spatially PCBs, and the B-integral is proportional to the decrease factor without considering the gain of the medium. The reference value of the source spatial coherence in the range with better B-integral suppression was characterized according to the ratio of the period of the fastest growing modulation to the spatial coherence length. The above findings provide theoretical guidance for nonlinear transmission in other types of media and have practical significance for the development of the spatially PCB laser driver and the assessment of its loading capacity.

## Acknowledgement

This work was supported by the Strategic Priority Research Program of the Chinese Academy of Sciences (Nos. XDA25020203 and XDA25020301).

## References

1. C. N. Danson and L. A. Gizzi, High Power Laser Sci. Eng. **11**, e40 (2023).
2. D. C. Brown, in *High-Peak-Power Nd: Glass Laser Systems* (Springer, Berlin, 1981), p. 188.
3. P. L. Bai, L. L. Fan, C. Fan, Z. B. Gan, L. L. Ji, Y. X. Leng, A. X. Li, S. Li, R. X. Li, X. Y. Liang, Y. Q. Liu, X. Y. Liu, C. Y. Qin, B. F. Shen, Y. J. Sun, Y. H. Tang, Q. S. Wang, N. W. Wang, C. Wang, X. L. Wang, X. B. Wang, T. J. Xu, Y. Xu, Z. Z. Xu, B. Yao, L. H. Yu, H. Zhang, Z. X. Zhang, and X. B. Zhang, High Power Laser Sci. Eng. **10**, e26 (2022).
4. N. Weiße, L. Doyle, J. Gebhard, F. Balling, F. Schweiger, F. Haberstroh, L. D. Geulig, J. Lin, F. Irshad, J. Esslinger, S. Gerlach, M. Gilljohann, V. Vaidyanathan, D. Siebert, A. Münzer, G. Schilling, J. Schreiber, P. G. Thirolf, S. Karsch, and A. Döpp, High Power Laser Sci. Eng. **11**, e44 (2023).
5. M. Bray and G. Chabassier, Proc. SPIE **3492**, 480 (1999).
6. M. Bray, A. Liard, and G. Chabassier, Proc. SPIE **3739**, 449 (1999).
7. M. D. Feit and J. A. Fleck, Jr. , J. Opt. Soc. Am. B **5**, 633 (1988).
8. V. I. Bespalov and V. I. Talanov, JETP Lett.-USSR **3**, 307 (1966).
9. A. J. Campillo, S. L. Shapiro, and B. R. Suydam, Bull. Amer. Phys. Soc. **18**, 1283 (1973).
10. E. S. Bliss, D. R. Speck, J. F. Holzrichter, J. H. Erkkila, and A. J. Glass, Appl. Phys. Lett. **25**, 448 (1974).
11. J. Garnier, Phys. Rev. E **73**, 046611 (2006).
12. S. Skupsky, R. W. Short, T. Kessler, R. S. Craxton, S. Letzring, and J. M. Soures, J. Appl. Phys. **66**, 3456 (1989).
13. L. Zhang, X. Fu, Z. Feng, H. Yang, and S. Wen, Sci. China Ser. G Phys. Mech. Astronomy **51**, 1653 (2008).
14. N. B. Baranova, N. E. Bykovskii, B. Y. Zel'dovich, and V. S. Yu, Sov. J. Quantum Electron. **4**, 1362 (1975).
15. Y. Zhang, X. Li, Y. Zhang, P. Sun, and J. Zhu, Chin. Opt. Lett. **8**, 210 (2010).
16. D. Auric and A. Labadens, Opt. Commun. **21**, 241 (1977).
17. I. V. Alexandrova, N. G. Basov, A. E. Danilov, S. I. Fedotov, Y. A. Mikhailov, and G. V. Sklizkov, Laser Particle Beams **1**, 241 (1983).
18. V. N. Alekseev, A. D. Starikov, A. V. Charukhchev, and V. N. Chernov, Kvantovaia Elektronika Moscow **6**, 1666 (1979).
19. U. Roth, F. Loewenthal, R. Tommasini, J. E. Balmer, and H. P. Weber, IEEE J. Quantum Electron. **36**, 687 (2000).
20. V. Ginzburg, E. Khazanov, A. Kochetkov, A. Kuzmin, V. Lozhkarev, S. Mironov, A. Prokhorov, I. Shaikin, A. Shaykin, S. Stukachev, and I. Yakovlev, High Power Laser Sci. Eng. **9**, e54 (2021).
21. Y. Zhu, Z. Zheng, X. Ge, G. Du, S. Ruan, C. Guo, P. Yan, P. Hua, L. Xia, and Q. Lü, Chin. Opt. Lett. **19**, 041403 (2021).
22. C. Liang, G. Wu, F. Wang, W. Li, Y. Cai, and S. A. Ponomarenko, Opt. Express **25**, 28352 (2017).
23. C. Liang, Y. E. Monfared, X. Liu, B. Qi, F. Wang, O. Korotkova, and Y. Cai, Chin. Opt. Lett. **19**, 052601 (2021).
24. Y. Shen, H. Sun, D. Peng, Y. Chen, Q. Cai, D. Wu, F. Wang, Y. Cai, and S. A. Ponomarenko, Appl. Phys. Lett. **118**, 181102 (2021).
25. D. Peng, Z. Huang, Y. Liu, Y. Chen, F. Wang, S. A. Ponomarenko, and Y. Cai, PhotoniX **2**, 6 (2021).
26. X. Lu, Y. Shao, C. Zhao, S. Konijnenberg, X. Zhu, Y. Tang, Y. Cai, and H. P. Urbach, Adv. Photonics **1**, 016005 (2019).
27. Y. Zhou, H. F. Xu, Y. Yuan, J. Peng, J. Qu, and W. Huang, IEEE Photonics J. **8**, 6600710 (2016).
28. Y. Liu, Y. Chen, F. Wang, Y. Cai, C. Liang, and O. Korotkova, Opto-Electron. Adv. **4**, 210027 (2021).

https://doi.org/10.1017/hpl.2024.12 Published online by Cambridge University Press

29. Y. Liu, X. Zhang, Z. Dong, D. Peng, Y. Chen, F. Wang, and Y. Cai, Phys. Rev. Appl. **17**, 024043 (2022).
30. T. Hansson, D. Anderson, M. Lisak, V. E. Semenov, and U. Österberg, J. Opt. Soc. Am. B **25**, 1780 (2008).
31. J. Hu, X. Ji, H. Wang, Y. Deng, X. Li, T. Wang, and H. Zhang, Opt. Express **29**, 23393 (2021).
32. J. T. Hunt, J. A. Glaze, W. W. Simmons, and P. A. Renard, Appl. Opt. **17**, 2053 (1978).
33. D. N. Christodoulides, T. H. Coskun, M. Mitchell, and M. Segev, Phys. Rev. Lett. **78**, 646 (1997).
34. M. Soljacic, M. Segev, T. Coskun, D. N. Christodoulides, and A. Vishwanath, Phys. Rev. Lett. **84**, 467 (2000).
35. X. M. Deng, X. C. Liang, Z. Z. Chen, W. Y. Yu, and R. Y. Ma, Appl. Opt. **25**, 377 (1986).
36. N. Fleurot, M. Andre, P. Estraillier, D. Friart, C. Gouedard, C. Rouyer, J. P. Thebault, G. Thiell, and D. Veron, Proc. SPIE **1502**, 230 (1991).
37. Y. Q. Gao, L. L. Ji, X. H. Zhao, Y. Cui, D. X. Rao, W. Feng, L. Xia, D. Liu, T. Wang, H. T. Shi, F. J. Li, J. Liu, P. Y. Du, X. L. Li, J. N. Liu, T. X. Zhang, C. Shan, Y. L. Hua, W. X. Ma, Z. Sui, J. Zhu, W. B. Pei, S. Z. Fu, X. Sun, and X. F. Chen, Opt. Lett. **45**, 6839 (2020).
38. P. Ma, B. Kacerovská, R. Khosravi, C. Liang, J. Zeng, X. Peng, C. Mi, Y. E. Monfared, Y. Zhang, F. Wang, and Y. Cai, Appl. Sci. **9**, 2084 (2019).
39. S. Basu, M. W. Hyde, X. F. Xiao, D. G. Voelz, and O. Korotkova, Opt. Express **22**, 31691 (2014).
40. X. H. Wang, J. H. Tang, Y. H. Wang, X. Liu, C. H. Liang, L. Zhao, B. J. Hoenders, Y. J. Cai, and P. J. Ma, Opt. Express **30**, 24222 (2022).
41. H. Lajunen, V. Torres-Company, J. Lancis, E. Silvestre, and P. Andrés, Opt. Express **18**, 14979 (2010).
42. F. Yang, G. Zhang, X. Zhang, Y. Zhang, R. Wang, and J. Zhu, Chin. Opt. Lett. **21**, 071901 (2023).
43. F. Gori and M. Santarsiero, Opt. Lett. **32**, 3531 (2007).
44. F. Gori, V. Ramírez-Sánchez, M. Santarsiero, and T. Shirai, J. Opt. A **11**, 85706 (2009).
45. R. Boyd, S. Lukishova, and Y. R. Shen, *Self-focusing: Past and Present: Fundamentals and Prospects* (Springer-Verlag, New York, 2009).
46. H. Nakano, N. Miyanaga, K. Yagi, K. Tsubakimoto, T. Kanabe, M. Nakatsuka, and S. Nakai, Appl. Phys. Lett. **63**, 580 (1993).
47. R. A. Shore, B. J. Thompson, and R. E. Whitney, J. Opt. Soc. Am. **56**, 733 (1966).

https://doi.org/10.1017/hpl.2024.12 Published online by Cambridge University Press